Kuramoto dynamics in Hamiltonian systems

Dirk Witthaut[1] and Marc Timme[1,2]

[1]*Network Dynamics, Max Planck Institute for Dynamics and Self-Organization (MPIDS), 37077 Göttingen, Germany*

[2]*Institute for Nonlinear Dynamics, Faculty of Physics, University of Göttingen, 37077 Göttingen, Germany*

(Received 9 January 2013; revised manuscript received 26 August 2014; published 19 September 2014)

The Kuramoto model constitutes a paradigmatic model for the dissipative collective dynamics of coupled oscillators, characterizing in particular the emergence of synchrony (phase locking). Here we present a classical Hamiltonian (and thus conservative) system with $2N$ state variables that in its action-angle representation exactly yields Kuramoto dynamics on N-dimensional invariant manifolds. We show that locking of the phase of one oscillator on a Kuramoto manifold to the average phase emerges where the transverse Hamiltonian action dynamics of that specific oscillator becomes unstable. Moreover, the inverse participation ratio of the Hamiltonian dynamics perturbed off the manifold indicates the global synchronization transition point for finite N more precisely than the standard Kuramoto order parameter. The uncovered Kuramoto dynamics in Hamiltonian systems thus distinctly links dissipative to conservative dynamics.

DOI: 10.1103/PhysRevE.90.032917 PACS number(s): 05.45.Xt

I. INTRODUCTION

Spontaneous synchronization constitutes one of the most prevalent order forming processes in Nature [1]. In 1975, Kuramoto introduced a now standard model of weakly coupled limit cycle oscillators to analyze synchronization processes [2]. The model characterizes the collective dynamics of a variety of dynamical systems ranging from chemical reactions [3] and neural networks [4] to coupled Josephson junctions [5], laser arrays [6], and optomechanical systems [7]. In the Kuramoto model, N phase oscillators are coupled via their phase differences. The rate of change of each phase ϕ_j is given by

$$\frac{d\phi_j}{dt} = \widetilde{\omega}_j + \sum_{\ell=1}^{N} \widetilde{K}_{j,\ell} \sin(\phi_\ell - \phi_j), \tag{1}$$

where ω_j is the intrinsic frequency of the jth oscillator, $j \in \{1,\ldots,N\}$, and $\widetilde{K}$ denotes the symmetric coupling matrix. Many studies deal with the important special case of a symmetric all-to-all coupling, i.e. $\widetilde{K}_{j,\ell} \equiv \widetilde{K}/N$ for all pairs (j,ℓ), and random frequencies drawn from a unimodal distribution $g(\omega)$. If $\widetilde{K}$ exceeds a certain threshold $\widetilde{K}_c$, this system exhibits a phase transition from an incoherent to a synchronous, phase-ordered asymptotic state in the thermodynamic limit $N \to \infty$. A second transition to a globally phase-locked state occurs for much stronger couplings (see, e.g., [8,9] and references therein). Despite its broad importance, many features of the Kuramoto model remain unknown. In particular, several of its relaxation and stability properties and the collective dynamics for finitely many coupled oscillators seem unusual for a dissipative system and are still not fully understood [10–15].

In this article, we introduce a class of (classical) Hamiltonian systems that exhibit a family of invariant tori on which the dynamics is identical to that of the Kuramoto model (1). This class of systems describes for instance the Lipkin-Meshkov-Glick (LMG) model in the thermodynamic limit [16] or the mean-field dynamics of a Bose-Einstein condensate (BEC) in a tilted optical lattice in certain parameter regimes [17,18]. After demonstrating mathematical equivalence of the Kuramoto and the Hamiltonian models on the invariant tori, we numerically and analytically study the full volume-preserving Hamiltonian dynamics, focusing on the onset of phase locking and its consequences. Intriguingly, the locking of the phase of one oscillator to the collective (average) phase implies the onset of transverse growth of that oscillator's action off the invariant tori. We derive an analytic expression quantifying the (phase) order parameter in terms of the local action instability. Beyond local dynamics, the deviation from the tori measured by the inverse participation ratio of the Hamiltonian system provides a distinguished indicator for the synchronization transition. It even scales more favorably with system size than the standard synchronization order parameter.

II. FUNDAMENTALS

Consider the Hamiltonian function

$$\begin{aligned}\mathcal{H}'(q_1,p_1,\ldots) = &\sum_{\ell=1}^{N} \frac{\omega_\ell}{2}\left(q_\ell^2+p_\ell^2\right) + \frac{L}{4}\left(q_\ell^2+p_\ell^2\right)^2 \\ &+ \frac{1}{4}\sum_{\ell,m=1}^{N} K_{\ell,m}(q_\ell p_m - q_m p_\ell) \\ &\times \left(q_m^2+p_m^2-q_\ell^2-p_\ell^2\right)\end{aligned} \tag{2}$$

defined on the N-particle phase space $\mathbb{R}^{2N}$ for local parameters ω_ℓ, L and symmetric coupling strengths $K_{m,\ell} = K_{\ell,m}$. The canonical transformation

$$I_\ell = \left(q_\ell^2+p_\ell^2\right)/2 \quad \text{and} \quad \phi_\ell = \arctan\left(q_\ell/p_\ell\right) \tag{3}$$

for $\ell \in \{1,\ldots,N\}$ simplifies the representation of the Hamiltonian in terms of action-angle variables I_ℓ and ϕ_ℓ for uncoupled harmonic ($K_{\ell,m} \equiv 0$ and $L = 0$) oscillators with single-particle Hamiltonian $\mathcal{H}'_\ell(q_\ell,p_\ell) = \omega_\ell(q_\ell^2+p_\ell^2)/2$. This transformation is invertible if and only if all $I_\ell > 0$, in particular if all $\mathcal{H}'_\ell > 0$. In the new action-angle variables $(\mathbf{I},\boldsymbol{\phi}) \in \mathbb{R}_+^N \times \mathbb{S}^N$, the Hamiltonian reads

$$\begin{aligned}\mathcal{H}(I_1,\phi_1,\ldots,I_N,\phi_N) = &\sum_{\ell=1}^{N} \omega_\ell I_\ell + L I_\ell^2 - \sum_{\ell,m=1}^{N} K_{\ell,m}\sqrt{I_m I_\ell} \\ &\times (I_m - I_\ell)\sin(\phi_m - \phi_\ell)\end{aligned} \tag{4}$$

and the equations of motion are given by

$$\dot{I}_j = -\frac{\partial \mathcal{H}}{\partial \phi_j} = -2\sum_{m=1}^{N} K_{m,j}\sqrt{I_m I_j}(I_m - I_j)\cos(\phi_m - \phi_j), \quad (5)$$

$$\dot{\phi}_j = \frac{\partial \mathcal{H}}{\partial I_j} = \omega_j + L I_j + \sum_{m=1}^{N} K_{m,j}[2\sqrt{I_j I_m}\sin(\phi_m - \phi_j). - \sqrt{I_m/I_j}(I_m - I_j)\sin(\phi_m - \phi_j)]. \quad (6)$$

One important property of these equations of motion is that they leave specific manifolds invariant. Any state with all actions homogeneous, $I_j \equiv I > 0$ for all j, yields $dI_j/dt = 0$ and thus leaves all actions unchanged. Thus the family of toric manifolds

$$T_I^N = \{(\mathbf{I},\boldsymbol{\phi}) \in \mathbb{R}_+^N \times \mathbb{S}^N \mid \forall j \in \{1,\ldots,N\} : I_j = I\} \quad (7)$$

are invariant under the flow generated by (5) and (6) for each given I. On one given torus, i.e., for one value of I, the dynamics of the phases

$$\dot{\phi}_j = \omega_j + LI + \sum_{\ell=1}^{N} 2I K_{\ell,j}\sin(\phi_\ell - \phi_j), \quad (8)$$

equals that of the original Kuramoto model (1) with a rescaled coupling matrix $\widetilde{K}_{j,\ell} = 2I K_{\ell,j}$ and shifted frequencies $\widetilde{\omega}_j = \omega_j + LI$. We conclude that the Hamiltonian function (2) generates the Kuramoto model on the invariant tori T_I^N. This holds for all symmetric coupling matrices and arbitrary frequency distributions.

The Hamiltonian dynamical system defined by (5), (6) has two constants of motion, the Hamiltonian function $\mathcal{H}$ itself and (twice) the total action

$$C^2 = \sum_{j=1}^{N}\left(p_j^2 + q_j^2\right) = 2\sum_{j=1}^{N} I_j. \quad (9)$$

The dynamics (5) is equivariant under a simultaneous scaling transformation $(p_j,q_j) \to (Cq_j,Cp_j)$ for all j and $K \to K/C^2$ for every $C > 0$, so we fix the normalization as $C^2 = N$ such that $\widetilde{K} = K$ without loss of generality and $I = 1/2$ defines the Kuramoto manifold $T_{1/2}^N$. Furthermore, the dynamics is equivariant with respect to a global phase shift, because it depends only on the phase differences. The two constants of motion and the shift-equivariance make the state space of the full Hamiltonian system effectively $(2N-3)$-dimensional, while the invariant subspace $T_{1/2}^N$ is an $(N-1)$-dimensional torus. In the following we drop the subscript $1/2$ for convenience.

III. ELEMENTARY MODEL SYSTEMS

What does the Hamiltonian dynamics tell us about the Kuramoto dynamics on the invariant manifold T^N? We first consider the simplest system with $N = 2$ units, which arises in the thermodynamic limit of the Lipkin-Meshkov-Glick model from nuclear physics [16]; see Appendix A 1 for details. The phase space structure of the Hamiltonian model is illustrated

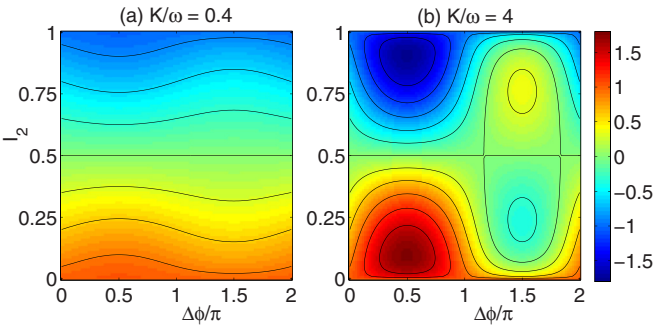

FIG. 1. (Color online) The full Hamiltonian dynamics for $N = 2$ coupled oscillators. Lines of constant energy of the Hamiltonian (2) for the frequencies $\omega_2 = \omega = -\omega_1$, $L = 0$ and coupling strength (a) below the critical one, $K < K_c = 2\omega$, and (b) above. points,

in Fig. 1 for two different values of the coupling strength. For $K := K_{1,2} = L = 0$, there are two elliptic fixed points off the Kuramoto manifold at $(I_1,I_2) = (0,1)$ at $(I_1,I_2) = (1,0)$. When K exceeds the critical coupling strength $K_c = |\omega_1 - \omega_2|$ two additional elliptic fixed points emerge off and two hyperbolic ("saddle") points on T^N via a Hamiltonian saddle node bifurcation. One of the hyperbolic fixed points corresponds to the phase-locked solution of the Kuramoto model. This phase-locked state is stable within T^N, but *unstable* transverse to it.

Systems with $N \geqslant 3$ show a much richer dynamics and suggest the emergence of chaos (cf. Fig. 2). Consider for instance three units with frequencies $(\omega_1,\omega_2,\omega_3) = (-2,-1,3)$. Whereas for small coupling, $K < K_{c1} \approx 1.5$, the Poincare section [19] indicates exclusively regular Hamiltonian dynamics [Fig. 2(a)], irregular dynamics [Fig. 2(c)] prevails for sufficiently large coupling, $K > K_{c2} \approx 4.6$, with mixed state space [Fig. 2(b)] for intermediate K. Simultaneous to the transitions in the full Hamiltonian system, synchronization appears on the Kuramoto manifold T^N as K increases. The oscillators 1 and 2 are unlocked for weak coupling and phase lock for $K > K_{c1}$, while the phase of the third oscillator remains incoherent. For $K > K_{c2}$, global phase locking sets in. For all $K \in [0,\infty)$, the dynamics is nonchaotic within the Kuramoto manifold (compare also to [20–22]).

Phase locking is indeed closely linked to the instability of the Hamiltonian action dynamics: For small coupling, where the Kuramoto dynamics is not phase locked, the actions exhibit stable dynamics [cf. Figs. 3(a) and 3(c)] and "action locking" $I_1 \approx I_2 \approx I_3 \approx 1/2$. In contrast, if the coupling is sufficiently strong such that oscillators lock their phases, the actions "unlock" and chaos manifests itself in intermittent bursts of the actions $I_j(t)$ [cf. Fig. 3(b) and 3(d)]. For intermediate coupling strengths, regular regions still exist around $\phi_2 - \phi_1 \approx 3\pi/2$ [indicated by the trajectories colored in blue and green in Fig. 2(b)] which confine the chaotic region around the torus T^N and lead to episodes of seemingly regular dynamics between the bursts.

IV. OSCILLATOR LATTICES

We further analyze the dynamics of a chain of oscillators with equidistant eigenfrequencies $\omega_n = \omega_B n$ and nearest-neighbor coupling, $K_{\ell,m} = K$ for $|\ell - m| = 1$ and zero

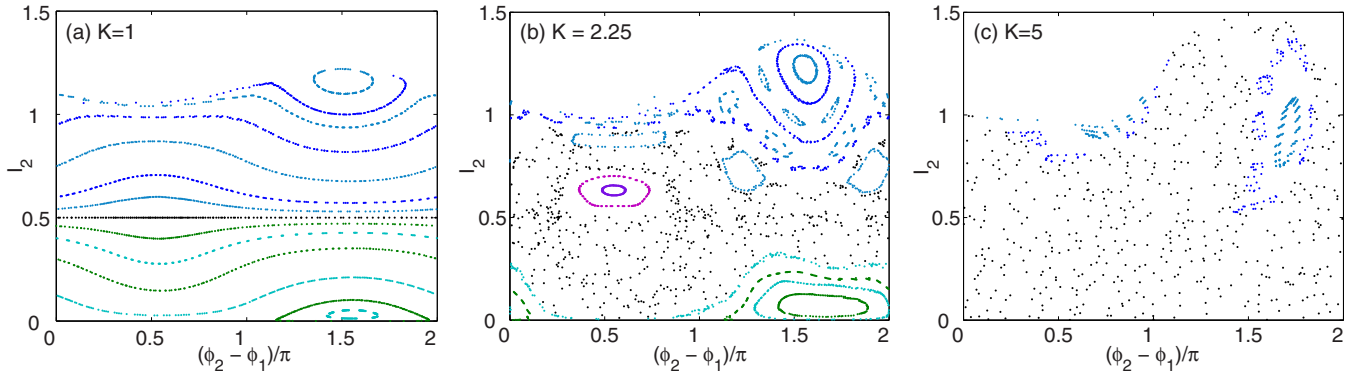

FIG. 2. (Color online) Emergence of chaos in the full Hamiltonian dynamics? Panels display two-dimensional Poincaré section of the phase space for $N = 3$, where the six-dimensional phase space reduces to effectively $2N - 3 = 3$ dimensions [19]. Different colors are used to guide the eye. The oscillator frequencies are $(\omega_1,\omega_2,\omega_3) = (-2,-1,3)$. (a) $K = 1 < K_{c1}$, (b) $K_{c1} < K = 2.25 < K_{c2}$, (c) $K = 5 > K_{c2}$.

otherwise. This system describes the dynamics of a Bose-Einstein condensate in a tilted optical lattice [17,18], which is a cornerstone model system for the study of nonlinear wave phenomena [23,24] and correlated quantum matter [25,26]. In a mean-field approximation, the condensate wave function evolves according to the nonlinear Schrödinger equation. Expanding the wave function into the localized eigenfunctions of the single-particle Schrödinger equation yields the Hamiltonian system (4) as shown in detail in Appendix A 2. In the noninteracting limit $K = L = 0$, all amplitudes rotate with with bare frequencies ω_j leading to periodic revivals which can be observed as Bloch oscillations [27–29]. The nonlinear mean-field potential leads to a density-dependent frequency shift (terms $\sim L$) and introduces a coupling of nearest-neighbor eigenstates (terms $\sim K$).

The dynamics in the vicinity of the Kuramoto manifold is particularly important for experiments as this corresponds to a homogeneous filling of the lattice. Weak nonlinearities disturb the strictly periodic dynamics, whereas actions remain "locked", $I_j \approx I_0$, as shown in Fig. 4. In experiments this leads to a damping of the atomic Bloch oscillations [18,30,31]. For stronger nonlinearities pairs of phases can lock, which implies that the actions I_j unlock such that density fluctuations start to grow exponentially as shown in Figs. 4(b) and 4(d). Synchronization in the form of phase locking thus implies the destruction of a Bose-Einstein condensate in a titled lattice.

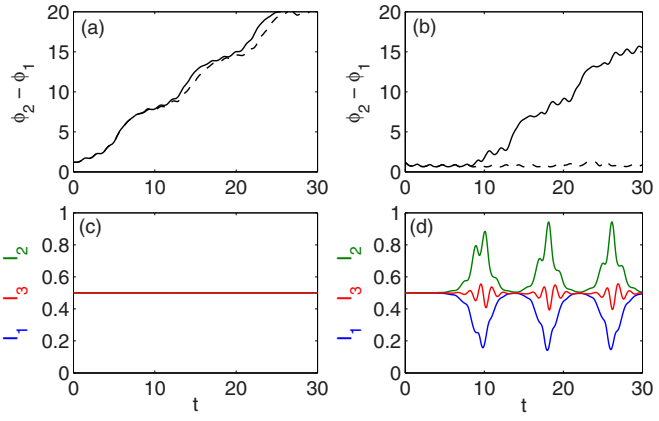

FIG. 3. (Color online) Action bursts indicate onset of synchrony. Panels show the dynamics of three coupled oscillators in the regime of (a,c) no phase locking and (b,d) partial phase locking. Solid lines show the dynamics of (a,b) the phases and (c,d) the actions $I_j(t)$. The initial state is drawn randomly by perturbing the actions $I_j(0)$ off the manifold $I_j \equiv 1/2$ by a random amount of the order of 10^{-4}; it is thus close to but not on T^N. Dashed lines show the dynamics of the phases $\phi_j(t)$ on the submanifold T^N, i.e., Kuramoto dynamics. Parameters are $(\omega_1,\omega_2,\omega_3) = (-2,-1,3)$ and (a,c) $K = 1$ and (b,d) $K = 2.25$, respectively.

V. THE SYNCHRONIZATION TRANSITION

The previous examples reveal the fundamental relation of synchronization in the Kuramoto model and the instability of the transverse dynamics: Stable synchronization of the Kuramoto dynamics implies that the phase space flow is contracting on the torus T^N. As the full Hamiltonian flow conserves the phase space volume, it must be expanding in

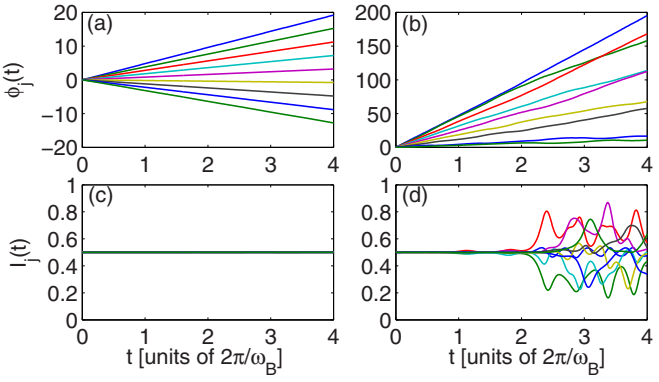

FIG. 4. (Color online) Dynamics of a chain of $N = 9$ oscillators with linearly increasing natural frequencies describing the mean-field dynamics of a BEC in a tilted optical lattice, in the regime of (a,c) no phase locking and (b,d) partial phase locking. The initial state is chosen as a homogeneous BEC with small density fluctuations, i.e., $I_j(0) = 1/2 + \epsilon_j$ with small random perturbations ϵ_j of the order 10^{-4}, and random phases $\phi_j(0)$. The initial state is thus close to but not on T^N. Parameters are $\omega_B = 0.25$ and (a,c) $K = 0.03$, $L = 0.4$ and (b,d) $K = 0.15$, $L = 2$ (cf. [17]).

directions transverse to T^N. These expansions are generally observed as bursts of the I_j [cf. Fig. 4(d)].

To quantitatively understand the relation between synchronization of the phases and the instablity of the actions, we consider the original version of the Kuramoto model with all-to-all coupling $K_{j,\ell} \equiv K/N$, $L = 0$, and frequencies drawn randomly from a Lorentzian distribution [2]. We analytically derive the approximate dynamics of perturbations

$$\epsilon_j(t) = I_j(t) - I_0 \tag{10}$$

off the torus T^N, where $I_0 = 1/2$ via action normalization. Expanding the equations of motion (5) to first order in ϵ_j (around $\epsilon_j \equiv 0$) yields the dynamics

$$\dot{\epsilon}_j = \sum_\ell A_{j,\ell}(t)\epsilon_\ell \,, \tag{11}$$

where $A_{j,\ell}(t) := \frac{K}{N}(\delta_{j,\ell}[\sum_m \cos(\phi_j - \phi_m)] - \cos(\phi_j - \phi_\ell))$. This expression directly links the action instability to the phase locking dynamics of the original Kuramoto model: For small perturbations ϵ_j, we approximate the dynamics of the phases $\phi_j(t)$ by the associated dynamics $\phi_j^T(t)$ on the Kuramoto manifold T^N. Assuming that the phase dynamics is fast, we further approximate $A_{j,\ell}(t)$ by its time-average

$$\overline{A}_{j,\ell} := \overline{\frac{K}{N}\,\delta_{j,\ell}\left[\sum_{m=1}^{N}\cos\left(\phi_j^T - \phi_m^T\right)\right] - \frac{K}{N}\cos\left(\phi_j^T - \phi_\ell^T\right)}. \tag{12}$$

The structure of the matrix $\overline{A}_{j,\ell}$ becomes particularly simple if N becomes large. The off-diagonal elements decay as $1/N$ such that the matrix tends to be diagonal. Carrying out the sum in the diagonal terms yields

$$\overline{A}_{j,\ell} = \delta_{j,\ell}\, K\, \overline{r\cos\left(\phi_j^T - \psi\right)} + \mathcal{O}\left(\frac{1}{N}\right), \tag{13}$$

with the order parameter [10,11]

$$re^{i\psi} = \frac{1}{N}\sum_{m=1}^{N} e^{i\phi_m^T}. \tag{14}$$

In general, if the phase of an oscillator j is not locked to the overall phase ψ, the cosine tends to average out (with time) such that $\overline{A}_{j,j} \approx 0$. In contrast, $\overline{A}_{j,j} > 0$ if the oscillator j is locked. Therefore we find that the perturbation $\epsilon_j(t)$ grow exponentially if and only if the corresponding phases are locked, at least for $N \gg 1$.

The numerical example shown in Figs. 5(a) and 5(b) illustrates this reasoning: Perturbations are particularly large, where the associated Kuramoto oscillators are phase locked (shaded regions). In particular, the fastest rate of divergence of the actions from the invariant manifold is expected for those oscillators that (i) are locked and (ii) are closest to the overall phase ψ (center of locking region) such that the cosine term is maximal.

The largest eigenvalue λ_1 of the matrix $(A_{j,\ell})_{j,\ell}$ dominates the rate of divergence of the actions for randomly chosen initial conditions close to the Kuramoto manifold. In the diagonal approximation (13) for $N \gg 1$ and assuming independence of r and $\cos(\phi_j^T - \psi)$ such that $\overline{r\cos(\phi_j^T - \psi)} = \overline{r} \times \overline{\cos(\phi_j^T - \psi)}$ and we obtain

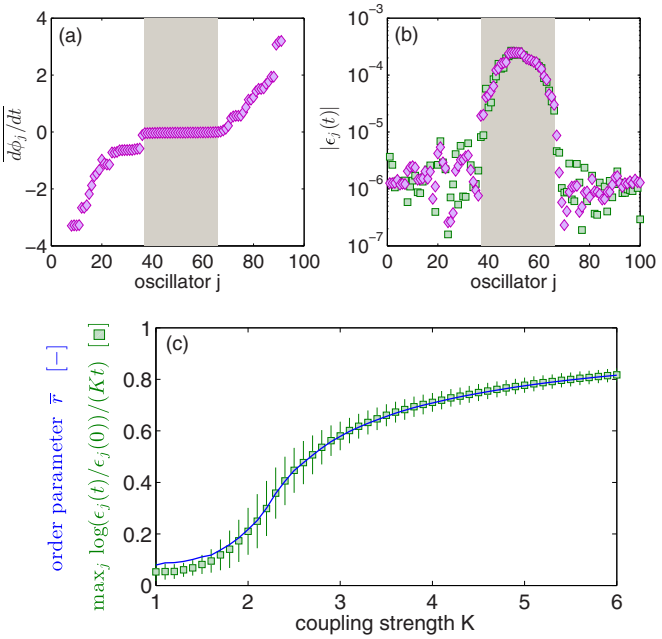

FIG. 5. (Color online) Transverse instability of actions predicts order parameter. (a) Average phase velocity $\overline{d\phi_j/dt}$ of $N = 100$ oscillators in the regime of partial phase locking at $K = 2.2$. (b) Perturbations $|\epsilon_j(t)|$ grow off the Kuramoto manifold, shown after $t = 10$, starting from $\epsilon_j(0) = \pm 10^{-6}$ with random signs. Exact numerical results for the Hamiltonian dynamics (□) are displayed in comparison to the diagonal approximation (11, 13), (◇). Actions grow substantially more for those oscillators that are phase-locked (shaded area). (c) The prediction of the order parameter from the Hamiltonian action dynamics (16) (□) well agrees with the actual order parameter r (14) (—) directly measured from the Kuramoto phases. [$N = 250$; data averaged over 100 realizations of the ω_j; vertical lines indicate standard deviation of (16)] [32].

$$\overline{r} \approx \frac{1}{K}\max_j \overline{A}_{jj} \tag{15}$$

because $\phi_j^T - \psi \approx 0$ for the j yielding the maximum and thus $\overline{\cos(\phi_j^T - \psi)} \approx 1$. This expression explicitly maps the stability properties of the actions to the locking properties of the phases. Thus the growth of the action perturbations in the full Hamiltonian system predicts the synchronization order parameter via

$$r \approx \frac{1}{Kt}\max_j \log[\epsilon_j(t)/\epsilon_j(0)]. \tag{16}$$

Direct observation of the order parameter from the Kuramoto phases shows excellent agreement [cf. Fig. 5(c)] with this prediction.

How can the instability be quantified beyond the linear approximation (11)? Again, we compare the dynamics on the Kuramoto manifold T^N (with initial actions $I_j(0) = 1/2$) with trajectories started in its immediate proximity (initial actions $I_j(0) = 1/2 + \epsilon_j$), and measure how much these dynamics deviate from each other by evaluating the variance of $(2I_j)$.

For this quantity, the inverse participation ratio, we find

$$\mathcal{P}_2 := \frac{\langle (2I_j)^2 \rangle_j - \langle 2I_j \rangle_j^2}{\langle 2I_j \rangle_j^2} = \frac{1}{N} \sum_{j=1}^{N} \left(p_j^2 + q_j^2\right)^2 - 1 \qquad (17)$$

due to action normalization. By construction, $\mathcal{P}_2 = 0$ on the torus T^N.

$\mathcal{P}_2 > 0$ indicates that the trajectory leaves the torus T^N and starts to burst. It is known that systems of Kuramoto oscillators exhibit a phase transition from an incoherent to a synchronized state at some K_c in the thermodynamic limit $N \to \infty$ [10]. For finite N, however, the transition is strongly blurred and the order parameter r increases smoothly with K (see also Fig. 6). Strikingly, the same transition in the full Hamiltonian system is substantially clearer as indicated by a sharp increase of the inverse participation ratio $\mathcal{P}_2 > 0$ from originally small values close to zero (Fig. 6). In fact, $\mathcal{P}_2$ indicates the transition more precisely than the Kuramoto order parameter, both with respect to the finite-size scaling below the transition and the jump occurring at the transition point K_c [see the insets of Figs. 6(b) and 6(c)].

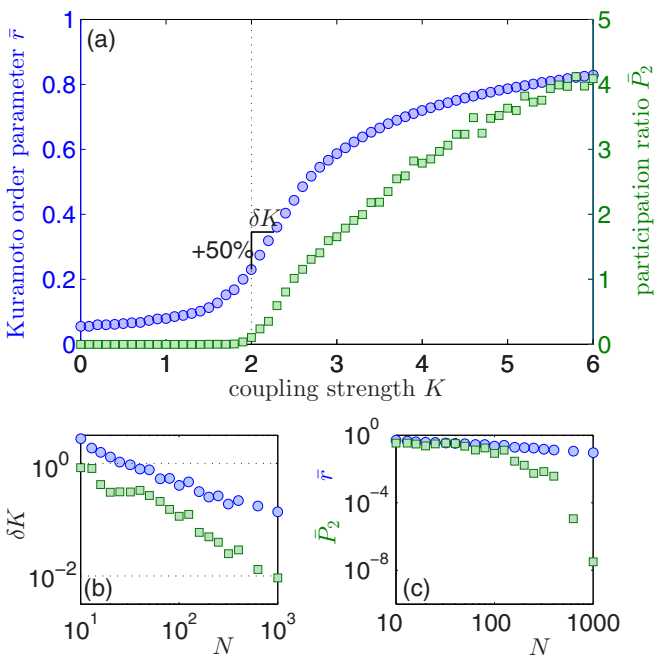

FIG. 6. (Color online) Inverse participation ratio of Hamiltonian dynamics reveals synchronization phase transition. (a) Order parameter $\bar{r}$ (○, left scale) and inverse participation ratio $\bar{\mathcal{P}}_2$ (□, right scale) as a function of coupling strength K for $N = 250$ oscillators. Mean-field theory predicts the onset of phase order in the Kuramoto model at $K_c = 2$ (dashed vertical line). (b) width of the transition region δK, where $\bar{r}$ increases by 50% from its critical value at K_c, i.e., $\bar{r}(K_c + \delta K) = 1.5\,\bar{r}(K_c)$ as a function of the number of oscillators N. (c) Finite size scaling of $\bar{r}$ and $\bar{\mathcal{P}}_2$ for a subcritical coupling strength $K = 1.8$. Initial actions are $I_j = 1/2$ (○) and $I_j = 1/2 + \epsilon_j$ (□), where the ϵ_j are drawn from a Gaussian distribution with standard deviation 10^{-4}. All data points are averages over 100 realizations each [32].

VI. SUMMARY

We have analytically and numerically demonstrated that a family of Hamiltonian systems bears the celebrated Kuramoto model of coupled oscillators as dynamics on its invariant (toric) manifolds T_I^N. Interestingly, the emergence of phase locking is equivalent to the emergence of a transverse instability off such a torus. An important consequence has been explicated for the dynamics of a Bose-Einstein condensate in a tilted optical lattice. The onset of phase locking between the lattice wells implies a dynamical instability and thus the destruction of the condensate. Moreover, studying the Hamiltonian systems can support our understanding of the collective dynamics of the Kuramoto model, in particular for finite N. The divergence of the actions quantifies the standard order parameter of the exact Kuramoto dynamics on T_I^N. The inverse participation ratio provides a distinguished indicator for the onset of transverse instability in the full Hamiltonian system and, consequently, the onset of synchronization of the Kuramoto phase dynamics.

ACKNOWLEDGMENTS

This work was partly supported by the Federal Ministry for Education and Research (BMBF Grant No. 03SF0472E to M.T. and D.W.), the Helmholtz Association (Grant No. VH-NG-1025 to D.W.), and the Max Planck Society (M.T.).

APPENDIX: PHYSICAL REALIZATIONS OF THE HAMILTONIAN SYSTEM

In this Appendix we provide details on the physical systems exhibiting the discussed Hamiltonian dynamics and discuss the occurrence of chaos. In Sec. A 1 we demonstrate how the Hamiltonian Kuramoto model with $N = 2$ oscillators arises in the thermodynamic limit of the longitudinal *Lipkin-Meshkov-Glick model.* This model was originally introduced in nuclear physics [16], and a variety of different experimental realizations have been propsed in recent years [33–35]. In Sec. A 2, we analyze the mean-field dynamics of Bose-Einstein condensates in tilted optical lattices described by the Gross-Pitaevskii or nonlinear Schrödinger equation [23,24]. Expanding the condensate wave function into the localized single-particle eigenstates yields the Hamiltonian model we introduced with a nearest-neighbor coupling [17,18].

1. Kuramoto dynamics in the themodynamic limit of the Lipkin-Meshkov-Glick model

The Lipkin-Meshkov-Glick (LMG) model is a standard model in statistical physics which was originally introduced to analyze shape transitions of atomic nuclei [16,36]. It describes N indistinguishable particles with two internal states, e.g., N hadronic spins or N two-level atoms. The particles interact symmetrically with each other and with an external magnetic field $\mathbf{h}$. The hamiltonian in its most general form is then given by

$$\hat{H} = \frac{1}{N}\left(\lambda_x \hat{S}_x^2 + \lambda_y \hat{S}_y^2\right) + h_z \hat{S}_z + h_y \hat{S}_y\,. \qquad (A1)$$

Traditionally, the case of a purely transversal field ($h_y = 0$) has received the most interest. However, a longitudinal field arises naturally in many quantum-optical realizations of the LMG model [33–35]. The LMG model is formulated in terms of the collective spin operators $\hat{S}_{x,y,z}$. The operator $\hat{S}_\pm = \hat{S}_x \pm \hat{S}_y$ generates (+) or annihilates (−) one collective spin excitation. The operator $\hat{S}_z$ is the population difference of excited and nonexcited spins or atoms, repectively. These operators form an angular momentum algebra with quantum number $N/2$,

$$[\hat{S}_a, \hat{S}_b] = +i\varepsilon_{a,b,c}\hat{S}_c,$$
$$\hat{S}_x^2 + \hat{S}_y^2 + \hat{S}_z^2 = \frac{N}{2}\left(\frac{N}{2}+1\right), \tag{A2}$$

where ε_{abc} is the totally asymmetric tensor. Using the conservation of the total angular momentum (A2) and rotating the coordinate system according to $\hat{S}_y = (\hat{S}'_z + \hat{S}'_y)/\sqrt{2}$ and $\hat{S}_z = (\hat{S}'_z - \hat{S}'_y)/\sqrt{2}$, the LMG Hamiltonian reads

$$H' = \frac{\lambda_y - 2\lambda_x}{2N}\left(\hat{S}'^2_y + \hat{S}'^2_z\right) + \frac{\lambda_y}{2N}(\hat{S}'_y\hat{S}'_z + \hat{S}'_z\hat{S}'_y) + \frac{h_y + h_z}{\sqrt{2}}\hat{S}'_z + \frac{h_y - h_z}{\sqrt{2}}\hat{S}'_y. \tag{A3}$$

up to a constant.

In the thermodynamic limit, the dynamics of the LMG model is equivalent to the Hamiltonian Kuramoto model introduced in the main text for the parameters

$$\lambda_y = 2\lambda_x =: -4K,$$
$$h_y = h_z =: \frac{\Delta\omega}{\sqrt{2}}. \tag{A4}$$

To show this we calculate the evolution equations for the expectation values $s_a = 2\langle\hat{S}'_a\rangle/N$ using Heisenberg equations. This yields

$$\dot{s}_x = -2K\left(s_z^2 - s_y^2\right) - \Delta\omega s_y - \frac{4K}{N}(C_{zz} - C_{yy}),$$
$$\dot{s}_y = -2K s_y s_x + \Delta\omega s_x - \frac{4K}{N}C_{xy}, \tag{A5}$$
$$\dot{s}_z = -2K s_x s_z - \frac{4K}{N}C_{xz}.$$

using units where $\hbar = 1$. In the thermodynamics limit $N \to \infty$ the terms including the covariances $C_{ab} := \frac{1}{N}\langle\hat{S}'_a\hat{S}'_b + \hat{S}'_b\hat{S}'_a\rangle - \frac{2}{N}\langle\hat{S}'_a\rangle\langle\hat{S}'_b\rangle$ can be neglected. Then we evolution equations close and we obtain a classical dynamical system. The equivalence to the Hamiltonian Kuramoto model can be seen explicitly by the parametrization of the Bloch vector,

$$\begin{pmatrix} s_x \\ s_y \\ s_z \end{pmatrix} = \begin{pmatrix} \sqrt{1-\Delta I^2}\cos(\Delta\phi) \\ \sqrt{1-\Delta I^2}\sin(\Delta\phi) \\ \Delta I \end{pmatrix}. \tag{A6}$$

One then finds the evolution equations for the paramters

$$\frac{d}{dt}\Delta\phi = \Delta\omega - 2K\sqrt{1-\Delta I^2}\sin(\Delta\phi) + 2K\frac{\Delta I^2}{\sqrt{1-\Delta I^2}}\sin(\Delta\phi), \tag{A7}$$
$$\frac{d}{dt}\Delta I = -2K\,\Delta I\sqrt{1-\Delta I^2}\cos(\Delta\phi).$$

These equations are equivalent to the Hamiltonian Kuramoto model with $N = 2$ oscillators and $L = 0$ introduced in the main text if we identify $\Delta I = I_2 - I_1$, $\Delta\phi = \phi_2 - \phi_1$, and $\Delta\omega = \omega_2 - \omega_1$.

2. Kuramoto dynamics of Bose-Einstein condensates in tilted optical lattices

Ultracold atoms in optical lattices provide a unique experimental system to study fundamental aspects of condensed matter physics [26], quantum-field theories [37–40], or nonlinear dynamical systems [23,24]. For very low temperatures and intermediate densities, bosonic atoms condense to a single quantum state (Bose-Einstein condensation), which can be described in a mean-field approximation. The dynamics of the order parameter or condensate wave function $\psi(x,t)$ is then described by the Gross-Pitaevskii or nonlinear Schrödinger equation (NLSE)

$$i\hbar\frac{\partial}{\partial t}\psi(x,t) = \left(-\frac{\hbar^2}{2m}\frac{\partial^2}{\partial x^2} + V(x) + g|\psi|^2\right)\psi(x,t). \tag{A8}$$

The atoms experience a nonlinear mean-field potential $g|\psi(x,t)|^2$, which is proportional to the density of the condensate. Here, we consider the case of an accelerated or tilted one-dimensional optical lattice,

$$V(x) = V_0\cos^2(kx) + Fx. \tag{A9}$$

The one-dimensional limit can be realized by a tight confinement of the atoms in the radial directions, while the external field F can be realized by accelerating the entire lattice [27], by gravity or by magnetic gradient fields [30,31]. A similar equation describes the light propagation in periodically structured nonlinear optical media [41].

The mean-field dynamics can be understood by expanding the wave function into the eigenstates of the linear system, the so-called Wannier-Stark resonance states [28,29]. The linear system has a fundamental symmetry: it is invariant under a combined translation by the lattice period $d = \pi/k$ and a shift of the energy by Fd. The eigenstates are therefore organized in ladders,

$$\Psi_{\alpha,n}(x) = \Psi_{\alpha,0}(x - dn),$$
$$E_{\alpha,n} = E_{\alpha,0} + dFn, \tag{A10}$$

where Ψ is the wave function and E the energy of the eigenstates. Each ladder $\alpha = 0,1,2,\ldots$ roughly corresponds to one Bloch band in the field-free case and $n \in \mathbb{Z}$ labels the rung of the ladder.

If the external field is not too strong, Landau-Zener tunneling between the bands can be neglected and the dynamics

takes place in the ground ladder $\alpha = 0$ only. Expanding the NLSE into the Wannier-Stark resonance states

$$\psi(x,t) = \sum_{n=-\infty}^{+\infty} c_n \Psi_{0,n}(x) \tag{A11}$$

then yields the equations of motion [17,18]

$$i\dot{c}_n = -\omega_n c_n + g \sum_{k,\ell,m} \chi_{k,\ell,m} c^*_{n+k} c_{n+\ell} c_{n+m}. \tag{A12}$$

The linear eigenfrequencies are equidistant,

$$\omega_n = -\omega_B\, n, \tag{A13}$$

where $\omega_B = dF/\hbar$ is the Bloch frequency, and the coupling coefficients are given by

$$\chi_{k,\ell,m} = \frac{1}{\hbar} \int_{-\infty}^{+\infty} \Psi^*_{0,0}(x) \Psi^*_{0,k}(x) \Psi_{0,\ell}(x) \Psi_{0,m}(x)\, dx. \tag{A14}$$

The dynamics becomes much simpler if the lattice is not too shallow. The Wannier-stark states $\Psi_n(x)$ are strongly localized such that only few of the coupling coefficients $\chi_{k,\ell,m}$ significantly differ from zero. The most important contributions are then given by the terms proportional to

$$g\chi_{0,0,0} =: -L,$$
$$g\chi_{0,0,+1} \approx -g\chi_{0,0,-1} =: -K$$

and all other contributions can be safely neglected. The evolution equations then read

$$\begin{aligned} i\dot{c}_n = &-\omega_n c_n - L|c_n|^2 c_n \\ &- K\big[(c^*_{n+1} - c^*_{n-1})c_n^2 + 2|c_n|^2(c_{n+1} - c_{n-1}) \\ &+ |c_{n-1}|^2 c_{n-1} - |c_{n+1}|^2 c_{n+1}\big]. \end{aligned} \tag{A15}$$

To further analyze this dynamics, we decompose the c_n into amplitude and phase according to

$$c_n = \sqrt{I_n} e^{i(\phi_n - n\pi/2)}. \tag{A16}$$

The additional constant phase shift $e^{-in\pi/2}$ has been introduced for notational convenience and has no physical consequences. This yields the equations of motion

$$\begin{aligned} \dot{I}_n = &-2K[\sqrt{I_{n+1}I_n}(I_{n+1} - I_n)\sin(\phi_{n+1} - \phi_n) \\ &+ \sqrt{I_{n-1}I_n}(I_{n-1} - I_n)\sin(\phi_{n-1} - \phi_n)], \end{aligned} \tag{A17}$$

$$\begin{aligned} \dot{\phi}_n = &\omega_n + LI_n + K[2\sqrt{I_{n+1}I_n}\sin(\phi_{n+1} - \phi_n) \\ &- \sqrt{I_{n+1}/I_n}(I_{n+1} - I_n)\sin(\phi_{n+1} - \phi_n) \\ &+ 2\sqrt{I_{n-1}I_n}\sin(\phi_{n-1} - \phi_n) \\ &- \sqrt{I_{n-1}/I_n}(I_{n-1} - I_n)\sin(\phi_{n-1} - \phi_n)]. \end{aligned} \tag{A18}$$

This is equivalent to the Hamiltonian system analyzed in the main text with equidistant frequencies defined by (A13) and nearest-neighbor coupling given by the coupling matrix

$$K_{\ell,m} = \begin{cases} K & \text{for} \quad |\ell - m| = 1, \\ 0 & \text{else.} \end{cases} \tag{A19}$$

This dynamical system becomes classically chaotic when the interaction strength increases as shown by Thommen *et al.* [17]. The authors show that chaos first appears for a very inhomogeneous filling, i.e., when the actions I_n differ significantly, and explain this scenario in terms of the Kolmogorov Arnold Moser (KAM) theorem. In the present paper we analyze the dynamics for a different scenario. The Kuramoto manifold defined by $I_n \equiv I$ corresponds to a homogeneous filling of the lattice, which is commonly realized in experiments.

The results presented in the main manuscript show that phase locking implies the transversal instablity of the Kuramoto manifold. For a Bose-Einstein condensate this corresponds to an unstable dynamics of the atomic density. Even more, a dynamical instability of the classical mean-field dynamics implies a dynamical instability of the underlying quantum dynamics, leading to an exponentially fast depletion of the condensate mode [42–44]. We thus conclude the following: Phase locking between different wells of the optical lattice implies the destruction of the Bose-Einstein condensate.

[1] A. Pikovsky, M. Rosenblum, and J. Kurths, *Synchronization: A Universal Concept in Nonlinear Sciences* (Cambridge University Press, Cambridge, England, 2003).

[2] Y. Kuramoto, in *International Symposium on Mathematical Problems in Theoretical Physics*, edited by H. Arakai, Lecture Notes in Physics Vol. 39 (Springer, New York, 1975).

[3] Y. Kuramoto, *Chemical Oscillations, Waves, and Turbulence* (Springer, Berlin, 1984).

[4] H. Sompolinsky, D. Golomb, and D. Kleinfeld, Proc. Natl. Acad. Sci. USA **87**, 7200 (1990).

[5] K. Wiesenfeld, P. Colet, and S. H. Strogatz, Phys. Rev. Lett. **76**, 404 (1996).

[6] A. G. Vladimirov, G. Kozireff, and P. Mandel, Europhys. Lett. **61**, 613 (2003).

[7] G. Heinrich, M. Ludwig, J. Qian, B. Kubala, and F. Marquardt, Phys. Rev. Lett. **107**, 043603 (2011).

[8] M. Verwoerd and O. Mason, SIAM J. Appl. Dyn. Syst. **10**, 906 (2011).

[9] F. Dörfler and J. Bullo, SIAM J. Appl. Dyn. Syst. **10**, 1070 (2011).

[10] S. H. Strogatz, Physica D **143**, 1 (2000).

[11] J. A. Acebron, L. L. Bonilla, C. J. Perez Vicente, F. Ritort, and R. Spigler, Rev. Mod. Phys. **77**, 137 (2005).

[12] Yu. Maistrenko, O. Popovych, O. Burylko, and P. A. Tass, Phys. Rev. Lett. **93**, 084102 (2004).

[13] H. Kori and A. S. Mikhailov, Phys. Rev. Lett. **93**, 254101 (2004).

[14] D. H. Zanette, Europhys. Lett. **68**, 356 (2004).

[15] C. Grabow, S. Hill, S. Grosskinsky, and M. Timme, Europhys. Lett. **90**, 48002 (2010).

[16] H. J. Lipkin, N. Meshkov, and A. J. Glick, Nucl. Phys. **62**, 188 (1965).

[17] Q. Thommen, J. C. Garreau, and V. Zehnlé, Phys. Rev. Lett. **91**, 210405 (2003).
[18] D. Witthaut, M. Werder, S. Mossmann, and H. J. Korsch, Phys. Rev. E **71**, 036625 (2005).
[19] I_2 is plotted vs $\phi_2 - \phi_1$ whenever the phase $\phi_3 - \phi_1$ crosses zero with $\dot{\phi}_3 - \dot{\phi}_1 > 0$. I_1 and I_3 are then fixed due to the conservation of total action C^2 and the total energy $\mathcal{H}$.
[20] S. Watanabe and S. H. Strogatz, Phys. Rev. Lett. **70**, 2391 (1993).
[21] E. Ott and T. M. Antonsen, Chaos **18**, 037113 (2008).
[22] C. Bick, M. Timme, D. Paulikat, D. Rathlev, and P. Ashwin, Phys. Rev. Lett. **107**, 244101 (2011).
[23] R. Carretero-Gonzalez, D. J. Frantzeskakis, and P. G. Kevrekidis, Nonlinearity **21**, R139 (2008).
[24] O. Morsch and M. Oberthaler, Rev. Mod. Phys. **78**, 179 (2006).
[25] I. Bloch, Nat. Phys. **1**, 23 (2005).
[26] I. Bloch, J. Dalibard, and W. Zwerger, Rev. Mod. Phys. **80**, 885 (2008).
[27] M. Ben Dahan, E. Peik, J. Reichel, Y. Castin, and C. Salomon, Phys. Rev. Lett. **76**, 4508 (1996).
[28] M. Glück, A. R. Kolovsky, and H. J. Korsch, Phys. Rep. **366**, 103 (2002).
[29] T. Hartmann, F. Keck, H. J. Korsch, and S. Mossmann, New J. Phys. **6**, 2 (2004).
[30] M. Gustavsson, E. Haller, M. J. Mark, J. G. Danzl, G. Rojas-Kopeinig, and H.-C. Nägerl, Phys. Rev. Lett. **100**, 080404 (2008).
[31] M. Gustavsson, E. Haller, M. J. Mark, J. G. Danzl, R. Hart, A. J. Daley, and H.-C. Nägerl, New J. Phys. **12**, 065029 (2010).
[32] In the simulations, we record $\bar{r}$, $\overline{\mathcal{P}}_2$, $\overline{A}_{j,\ell}$, and $\overline{d\phi_j/dt}$ averaged over a time interval $\Delta t_2 = 10$, after an initial transient period of length $\Delta t_1 = 10$. The initial ϕ_j are randomly drawn from the uniform distribution on $[0,2\pi)$, but the same for perturbed and unperturbed actions. In Fig. 5(b), we use phases ϕ_j^T after the transient as initial values. In Fig. 5(c), we integrate the Hamiltonian dynamics up to a time t for which $\max_j |\epsilon_j(t)| \geqslant 10^{-4}$. The frequencies ω_j are drawn from a Cauchy distribution with density $g(\omega) = (a/\pi)/(\omega^2 + a^2)$ and width $a = 1$.
[33] R. G. Unanyan and M. Fleischhauer, Phys. Rev. Lett. **90**, 133601 (2003).
[34] G. Chen, J. Q. Liang, and S. Jia, Opt. Express **17**, 19682 (2009).
[35] J. Larson, Europhys. Lett. **90**, 54001 (2010).
[36] S. Dusuel and J. Vidal, Phys. Rev. Lett. **93**, 237204 (2004).
[37] K. Osterloh, M. Baig, L. Santos, P. Zoller, and M. Lewenstein, Phys. Rev. Lett. **95**, 010403 (2005).
[38] J. I. Cirac, P. Maraner, and J. K. Pachos, Phys. Rev. Lett. **105**, 190403 (2010).
[39] D. Witthaut, T. Salger, S. Kling, C. Grossert, and M. Weitz, Phys. Rev. A **84**, 033601 (2011).
[40] T. Salger, C. Grossert, S. Kling, and M. Weitz, Phys. Rev. Lett. **107**, 240401 (2011).
[41] R. Morandotti, U. Peschel, J. S. Aitchison, H. S. Eisenberg, and Y. Silberberg, Phys. Rev. Lett. **83**, 4756 (1999).
[42] Y. Castin and R. Dum, Phys. Rev. Lett. **79**, 3553 (1997).
[43] F. Trimborn, D. Witthaut, and H. J. Korsch, Phys. Rev. A **77**, 043631 (2008).
[44] F. Trimborn, D. Witthaut, and H. J. Korsch, Phys. Rev. A **79**, 013608 (2009).